Glycoconj J (2007) 24:449–464
DOI 10.1007/s10719-007-9037-0

NMR studies on the conformation of oligomannosides and their interaction with banana lectin

Caroline Clavel · Angeles Canales · Garima Gupta · J. Ignacio Santos · F. Javier Cañada · Soledad Penadés · Avadesha Surolia · Jesús Jiménez-Barbero

Received: 19 September 2006 / Revised: 22 February 2007 / Accepted: 4 April 2007 / Published online: 11 May 2007

Abstract The conformational and dynamic behaviour of three mannose containing oligosaccharides, a tetrasaccharide with α1→2, and α1→3, and a penta and a heptasaccharide with α1→2, α1→3, and α1→6 linkages has been evaluated by molecular mechanics and dynamics simulations and NMR spectroscopical methods. It is found that they display a fair amount of conformational freedom, with one major and one minor conformation per glycosidic linkage. The evaluation of their recognition by banana lectin has also been performed by STD NMR methods and a preliminary view of their putative interaction mode has been carried out by means of docking procedures.

Keywords Mannose oligosaccharides · NMR · Molecular dynamics · Banana lectin · Molecular recognition

C. Clavel · S. Penadés
Laboratory of Glyconanotechnology, CIC biomaGUNE,
Paseo Miramón 182.,
20009 San Sebastián, Spain

S. Penadés
e-mail: spenades@cicbiomagune.es

A. Canales · J. I. Santos · F. J. Cañada · J. Jiménez-Barbero (✉)
CIB-CSIC,
Ramiro de Maeztu 9,
28040 Madrid, Spain
e-mail: jjbarbero@cib.csic.es

G. Gupta · A. Surolia
Indian Institute of Science,
Bangalore 560 012, India

A. Surolia
e-mail: surolia@mbu.iisc.ernet.in

Introduction

Multivalent carbohydrate binding by lectins is critical for bacterial and viral adhesion and cancer metastasis [1]. Indeed, the presence and recognition of high-mannose-type oligosaccharides has been shown to play a key role in protein quality control, with several intracellular proteins, such as lectins, chaperones and glycan-processing enzymes, being involved in this process [2]. In particular, a broad range of proteins bind the high-mannose carbohydrates found on the surface of the HIV-associated envelope glycoprotein, gp120, and thus interfere with the viral life cycle, providing a potential new way of controlling infections, including HIV [3]. These proteins are thought to recognize the high-mannose-type glycans with subtly different structures, although the precise specificities are yet to be clarified. In order to gain a clear understanding of these protein–carbohydrate recognition processes and on the way of controlling them, the access to well defined mannose-containing oligosaccharides by means of organic synthesis is of paramount importance [4, 5]. In addition, it is advisable to provide these oligosaccharides with the possibility of forming part of multivalent entities, forming part of saccharide-containing clusters [6]. Indeed, it has been demonstrated that synthetic oligomannose clusters could mimic some of these carbohydrate epitopes (also including those of the 2G12 antibody), providing antigenicity [7]. Recently, gold glyconanoparticles (GNPs) have been prepared as new multivalent tools that mimic carbohydrate presentation on the cell surface. GNPs are highly soluble under physiological conditions, stable against enzymatic degradation and non-toxic [8, 9]. Therefore, GNPs are adequate tools for basic studies in carbohydrate interactions and for intervention in biological processes [10, 11].

Obviously, there are key implications of the precise three-dimensional structure and dynamics of the oligosaccharides in the recognition process and that knowledge is critical for controlling these events [12]. Thus, as part of a project devoted to the synthesis, interaction studies and applications of gold glyconanoparticles [13], we herein present the conformational study of three linear and branched oligomannosides containing 1→2, 1→3, and 1→6 linkages. These molecules have been prepared as components of mannose-containing GNPs as potential microbicides that could block HIV-1 gp120 binding to DC-SIGN. We also report a preliminary study of their interaction with Banana lectin (Banlec), a dimeric plant lectin from the jacalin-related lectin family, used as a model [14]. It is widely recognized that plant lectins are excellent model systems for the study of protein–carbohydrate interactions because of their robustness and ready availability [15]. Moreover, lectins of the jacalin family have been speculated to be involved in the interaction with gp120 glycoprotein [3].

Experimental

Compounds

The studied oligosaccharides have been prepared with good yields with a minimal number of building blocks, following the one-pot self-condensation synthesis described by Wong and coworkers [16]. The synthesis will be reported elsewhere. Banana lectin was isolated and purified as previously described [14].

NMR

NMR spectra of compounds **1–3** were recorded in D_2O at 500 MHz on a Bruker AVANCE spectrometer at 298–300 K. The ^1H and ^{13}C NMR spectra of **1–3** were assigned employing a combination of 2D-TOCSY [17], NOESY [18], T-ROESY [19], HSQC [20] and HSQC-TOCSY experiments.

The T-ROESY and NOESY experiments were performed in the phase-sensitive mode with the TPPI method for quadrature detection in F1. Typically, a data matrix of 2K× 512 points was employed to digitize a spectral width of 4,000 Hz. Thirty-two to forty-eight scans were used per increment with a relaxation delay of 2 s. Prior to Fourier transformation, zero filling was performed in F1 to expand the data to 4K×2K. Baseline correction was applied in both dimensions. Selective 1D and 2D-NOESY and T-ROESY experiments in D_2O were carried out with mixing times of 100, 200, 300, 400, 500, 600 and 700 ms. NOE contacts are collected in the Tables.

The selective experiments were recorded employing a double pulse field gradient spin echo (DPFGSE) module [21]. NOE intensities were normalized with respect to the diagonal peak at zero mixing time. Selective T_1 measurements were performed on the anomeric and several other protons to obtain the above-mentioned values. Experimental NOEs were fitted to a double exponential function, $f(t)=p0(e^{-p1t})(1-e^{-p2t})$ with p0, p1 and p2 being adjustable parameters [22]. The initial slope was determined from the first derivative at time $t=0$, $f'(0)=p0p2$. From the initial slopes, interproton distances were obtained by employing the isolated spin pair approximation.

HSQC experiments were carried out in order to obtain the complete ^1H and ^{13}C assignment. A data matrix of 1K× 1K was used to digitize a spectral width of 4,000 Hz in F_2 and 12,500 Hz in F_1. Thirty-two scans were used per increment with a relaxation delay of 1 s and a delay corresponding to a J value of 145 Hz. ^{13}C decoupling was achieved by the WALTZ scheme. HSQC-TOCSY experiments employed the same conditions including a 50 ms MLEV16 isotropic mixing time.

Chemical shifts and coupling constants are reported in the supporting information section.

STD experiments [23] were performed without saturation of the residual HDO signal for molar ratios between 15:1 and 50:1 of compound/protein. A train of Gaussian-shaped pulses of 50 ms each was employed, with a total saturation time of the protein envelope of 2 s and a maximum B1 field strength of 60 Hz. An off-resonance frequency of $\delta=40$ ppm and on-resonance frequencies between $\delta=-1.0$ ppm (protein aliphatic signals region) were applied. In all cases, line broadening of ligand protons was monitored. The STD experiments were repeated twice, with different batches of the lectin. Basically, similar results were obtained in both sets. In each case, the intensities were normalized (Table 4) with respect to the highest response, which always corresponded to one of the H-2 protons.

Molecular mechanics and dynamics calculations

All calculations were performed using the MacroModel/Batchmin [24] package (version 7.0) and the MM3* force field [25]. Charges were taken from the force field (all-atom charge option) and water solvation was simulated using MacroModel's generalized Born GB/SA continuum solvent model [26].

The torsion Φ angles [27] are defined as $H1_{ManA}$–$C1_{ManA}$–O–CX_{ManB} and Ψ as HX_{ManB}–CX_{ManB}–O–$C1_{ManA}$, for both 1→2 and 1→3 linkages. For the 1→6 linkage, Ψ is $C5_{Man}$–$C6_{Man}$–O–$C1_{Man}$. The torsion angle around the C5–C6 linkage (ω) is defined as O5–C5–C6–O6. Two different conformers were considered gt (ω +60°), and gg (ω −60°).

The numbering of the different oligosaccharides is given in the corresponding schemes.

All the different possible staggered conformers around all the glycosidic angles (and ω for the 1→6 linkage) were generated and optimized with MM3*. The GB/SA solvation model for water was used. The probability distribution was calculated from the energy values according to a Boltzmann function at 300 K.

In addition, a conformational search procedure was carried out using 15,000 steps of the Macromodel MC procedure. Again, the Φ and Ψ linkages, and the C5–C6 bonds were used as explicit variables during the Monte Carlo search. Extended nonbonded cut off distances (a van der Waals cut off of 8.0 Å and an electrostatic cutoff of 20.0 Å) were used. The interatomic distances r reported in the Tables under the MC/EM and MD header are averaged between those calculated from a Boltzmann $< r_i^{-6} >$ average of the MC search and those estimated by $< r_i^{-6} >$ averaging of the snapshots saved during the MD simulations.

The MD simulations were run using the MM3* force field and van der Waals and electrostatic cutoffs of 25 Å, together with a hydrogen bond cutoff of 15 Å. All simulations were performed at 300 K, with a time step of 1.5 fs. Runs of 5 ns each were performed, starting from different conformations of the molecules, selected from the MC outputs, which differed at glycosidic linkage. Structures were sampled every 5 ps and saved for later evaluation.

Docking The different stable conformers of **1**, **2**, and **3** were manually docked on both active binding site of banana lectin by superimposing the terminal (reducing or non-reducing) residues of the corresponding penta- or heptasaccharide molecules on the existing mannose moieties of the two deposited Man/lectin and XylMan complexes (pdb codes, 1X1V and 2BN0, respectively in references 37 and 38). For the tetrasaccharide, docking of the four residues was alternatively attempted at both binding sites. No minimization was performed. Those solutions that led to steric hindrance or clashing were discarded.

Results and discussion

The three synthetic oligosaccharides studied herein show structural features also present in the $Man_9GlcNAc_2$ oligosaccharide, although they may be considered as fragments or non-natural modifications thereof. Therefore, several experimental data on the structure and conformational behaviour of the natural complete oligosaccharide and fragments thereof are available from X-ray crystallography and NMR spectroscopy [28, 29]. Computational studies have also been described for the (1→2) and (1→6) linked mannotrioside, using molecular mechanics and dynamics simulations [30]. These latter studies suggested little correlation between the motion of the two glycosidic linkages, (1→2) and (1→6), which indeed behaved as they do in the respective (1→2) and (1→6) linked dimannosides [31].

Therefore, for the study of these new oligosaccharides **1**–**3**, a similar protocol to that used for the basic trisaccharide 4 has been adopted.

The analysis will be described independently for the tetra- (1), penta- (2) and the hepta- (3) oligosaccharides (Scheme 1).

The tetrasaccharide (1)

The manual and Monte Carlo conformational search yielded eight conformational families, whose low-energy conformers are within 10 $kJmol^{-1}$ from the global minimum (Table 1). These conformations mainly differed for the value of $\Psi_{1\to3}$ and $\Psi_{1\to2}$ torsion angles (Fig. 1). These structures were used as the starting point of eight separated 3 ns MD runs. The collected output of the dynamic simulations (24 ns simulation total, MC/SD set of Table 1) as well as the representative conformers were compared with those obtained through NMR data by using 1D and 2D-NOESY and T-ROESY spectra acquired at different mixing times on a 500 MHz spectrometer.

The conformation and dynamics of the Manα1→2-Man and Manα1→3-Man linkages has been studied extensively in oligomannoses, $Man_nGlcNAc_2$. Although in principle, one conformer seemed to comply with the experimental data [32], more recent computational [33] and experimental [34] results suggest that these linkages exist in two distinct, flexible conformations with similar Φ value, in agreement with the exo-anomeric effect (ca. $-45\pm15°$) and different interconverting Ψ values in the positive and negative ranges. In fact, transitions between the two conformations are observed in the MD simulations starting from any of the conformers. The two conformations are represented in available X-ray structures of mannose oligosaccharides and account for the set of three NOE contacts typically observed across the glycosidic linkage [35]. For the Manα1→2-Man, the H1–H1′ contact can only arise from positive Ψ conformers, the H5′–H1 one only from negative Ψ geometries. The other observed NOE contact belongs to the interglycosidic H1′–H2 pair, which is at NOE distance in both conformations. For the Manα1→3-Man glycosidic linkage, the H2–H5′ contact may be displayed for both positive and negative Ψ geometries, while the H1′–H2 one only from positive-Ψ geometries. Other observed NOE is the interglycosidic H1′–H3 pair, again at NOE distance in both conformations.

Scheme 1 The three oligosaccharides studied herein. From top to bottom, **1**, **2**, and **3**

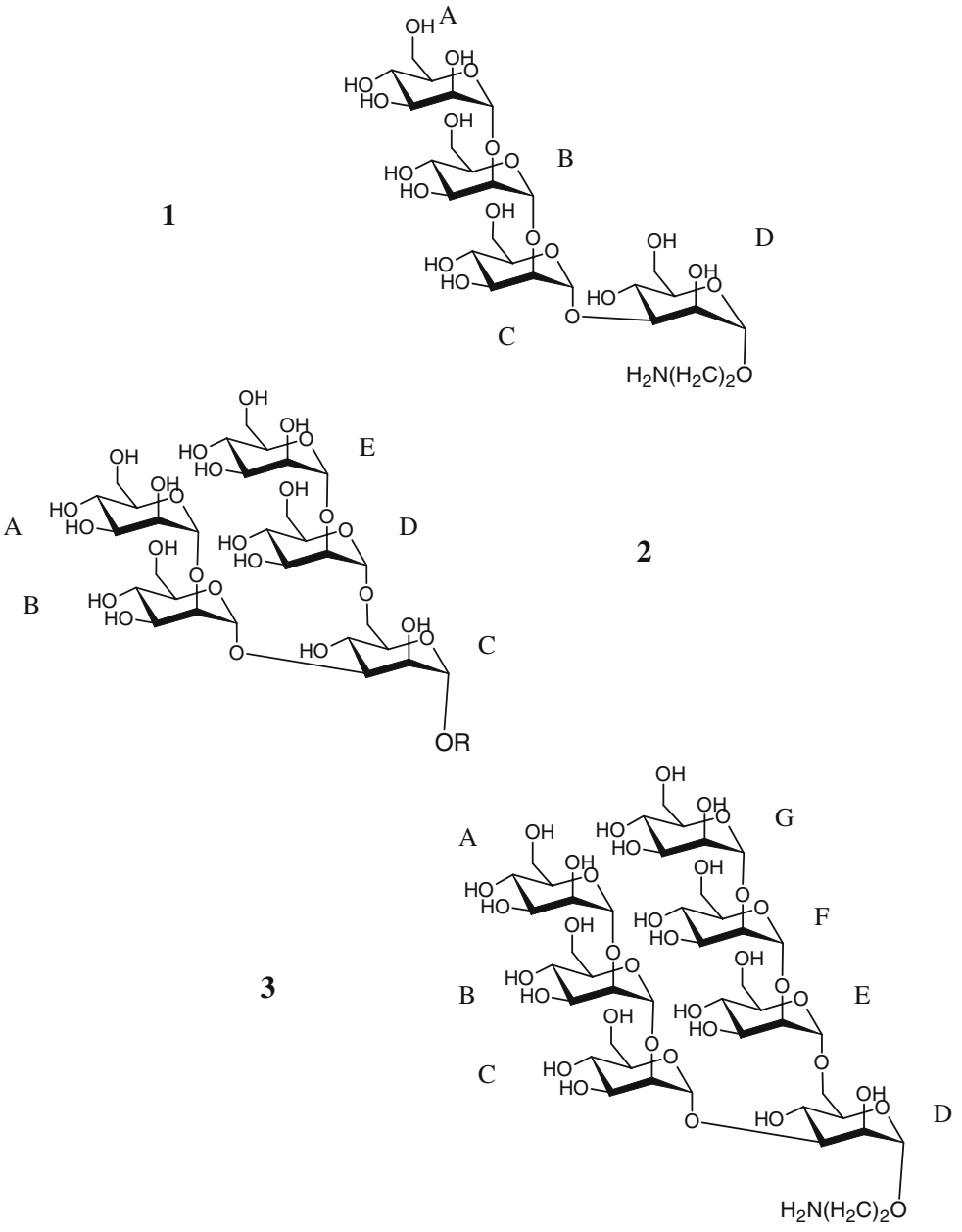

The α-Man-(1→2)- α-Man-linkage

Tetrasaccharide **1** displays two Manα1→2-Man linkages, dubbed ManAα1-2-ManB and ManBα1→2-ManC. According to the modelling procedure, the negative Ψ conformation (Φ, Ψ −55°, −22°) is slightly preferred over the positive one (Φ, Ψ −33°, 57°) for both glycosidic linkages, with a preference around 1.5:1. Indeed, a continuum motion between the conformers is observed in the MD runs (Fig. 3a). The relation between NOE signals and proton–proton distances is well established and can be worked out at least in a semi-quantitative manner using an interproton relaxation matrix [36].

The NOE intensities reflect the conformer population, and therefore by focusing on the key, mutually exclusive NOE interactions, is possible to characterize the different conformations (Table 1, Fig. 1). For both Manα1→2-Man linkages, the observed H5′–H1 NOE intensity is always more intense than the corresponding H1′H1. These observations indicate that the conformational equilibrium in water solution favours the negative-Ψ conformer (extended geometry) over the positive one (stacked geometry) for both the terminal non-reducing and the central glycosidic linkages. A 30:70 distribution between the positive and negative-Ψ conformers, instead of the 40:60 MM3*-predicted one, quantitatively accounts for the observed NOEs.

Table 1 Calculated and experimental interproton distances (Å) for **1** and the observed NOE contacts

Linkage	Proton pair	Average distance (Å)[b]	Exp. Distances (Å) (ISPA model)[c]	NOE intensity (NOE/t-ROE)	Distances (Å) for conformers[d] stacked-Ψ/extended-Ψ
α1→2	H_1'–H_1	AB[a] 2.9	AB[a] 3.2	Weak	2.6/4.3
	H_1'–H_1	BC[a] 3.0	BC[a] 3.3	weak	
	H_1'–H_2	AB 2.3	AB 2.4	Strong	2.2/2.6
	H_1'–H_2	BC 2.4	BC 2.4	strong	
	H_5'–H_1	AB 2.5	AB 2.5	strong-med	3.6/2.3
	H_5'–H_1	BC 2.5	BC 2.5	strong-med	
	H_5'–H_2	AB 3.4	not detected	not detected	4.4/3.0
	H_5'–H_2	BC 3.2			
α1→3	H_1'–H_3	CD[a] 2.4	CD[a] 2.3	strong	2.2/2.5
	H_1'–H_2	CD 3.2	CD 3.2	weak	2.6/4.1
	H_5'–H_2	CD 2.6	CD 2.5	medium	3.2/2.3

[a] AB and BC stand for the two Manα1→2Man linkages; CD refers to the Manα1→3Man linkage of **1**. In all cases, the corresponding non-reducing moiety of a given linkage is primed.
[b] Averaged distances calculated from the $\langle r^{-6} \rangle$ ensembles estimated as described in the experimental section.
[c] Distances for compound **1** were derived using the isolated spin-pair approximation (ISPA) according to the protocol described in the experimental section from 1D, 2D NOESY and T-ROESY data. Error estimation in the measurement are smaller than 0.2 Å.
[d] Estimated distances for the representative stacked (positive-Ψ) and extended (negative-Ψ) conformers for both Manα1→2Man and Manα1→3Man.

The α-Man-(1→3)- α-Man linkage

In this case, the negative Ψ geometry (Φ, Ψ −33°, 57°) is preferred over the positive one (Φ, Ψ −55°, −22°), with a preference around 4:1. These expectations are indeed satisfied by the NMR data. When considering the exclusive NOEs (Table 1), The H5′–H2 NOE intensity is always more intense (estimated distance 2.5 Å) than the corresponding H1′–H2 (estimated distance 3.0 Å). These observations indicate that the conformational equilibrium in water solution favours the negative Ψ conformer over the positive one with a 70:30 distribution.

Thus, the conformational behaviour of **1** may be described by a distribution of conformers, which display exo-anomeric conformations around all the Φ angles of the molecule and fluctuations around the Ψ glycosidic linkages, preferably centered around negative Ψ-values, but also fluctuating towards positive values. A superimposition of different representative conformers is given in Fig. 1, which also contains the superimposition of 100 snapshots from the MD simulations.

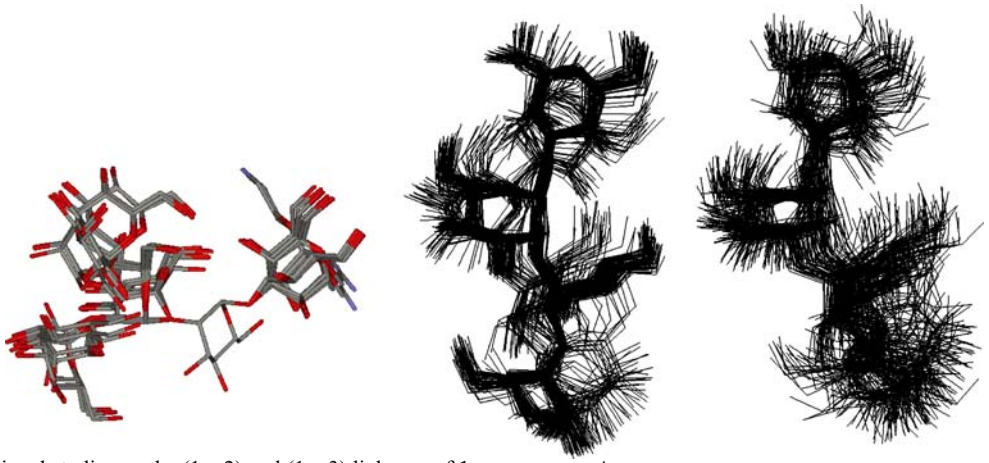

Fig. 1 Conformational studies on the (1→2) and (1→3) linkages of **1**. ***Left***. Superimposition of the eight representative geometries that encompasses the possible conformational space available to **1**. Residue C has been chosen for superimposition. Distances between the O4 atoms of residues A and D vary between 7.2 and 11.2 Å, thus indicating the existence of stacked-like and extended conformers. $\Phi_{1\to2}$: H1′–C1′–O–C2; $\Psi_{1\to2}$: C1′–O–C2–H2. $\Phi_{1\to3}$: H1′–C1′–O–C3; $\Psi_{1\to3}$: C1′–O–C3–H3. Calculations were run with MMOD 7.0, using MM3* and the GB/SA water solvation model. ***Middle***—5 ns of MC/SD dynamics simulation starting from the positive Ψ torsion angle. ***Right***—5 ns of MC/SD dynamics simulation starting from the negative Ψ torsion angle. In all cases, the conformational flexibility may be appreciated

The individual representations of the eight representative conformational families are gathered in the supporting information.

The pentasaccharide (2)

The conformational search yielded 16 conformational families within 15 kJmol^{-1} from the global minimum (see Table 2). For **2**, there is one additional degree of freedom for the $\omega_{1\rightarrow6}$ torsion. Again, these structures were used as the starting point of sixteen separated 2 ns MC/SD dynamic runs. The collected output of the dynamic simulations (32 ns simulation total, MC/SD set of Table 1) as well as the representative conformers were compared with those obtained through NMR as described for **1**.

The conformation and dynamics of the Manα1→6-Man linkages has also been studied extensively in $Man_9GlcNAc_2$ and shorter oligosaccharides. This linkage usually populates a single conformation of Φ, centered around −60°; two differently populated states for Ψ, a major one around 180° and a minor one with a value of 90° and two values for ω (*gt*, ω=60°, *gg*, ω=−60°), whose respective populations depend on the degree of branching [37].

Pentasaccharide **2** displays two Manα1→2-Man linkages, dubbed ManAα1-2-ManB and ManEα1→2-ManD. For **2**, the negative Ψ conformation is again preferred over the positive one for both glycosidic linkages, with a similar preference to that described above (Fig. 2). The Manα1→3-Man also displays a similar behaviour to that detailed for **1**, indicating that the correlation between the motion around the Manα1→3-Man (between units B and C) and Manα1→6-Man (between units D and C) linkages is small.

The simulations of **2** produced a complex picture of its conformational behaviour. Besides the equilibrium between the positive and negative Ψ values around the Manα1→3-Man and Manα1→2-Man linkages, the Manα1→6-Man moiety displays additional flexibility with exchange between two ω conformers, namely *gg* and *gt*. Therefore, **2** seems to be a very flexible moiety (the details have been collected in the Supplementary data section). According to the simulations, the *gg* cluster may be correlated with the presence of positive type conformers for Ψ of the (1→2) linkage. The Ψ_{1-6} torsion is mainly represented by an anti-type conformer, with ca. 180°, and with minor contributions for gauche-type geometries.

The exclusive NOEs described above may be used to assess their presence in the conformational equilibrium. The interatomic distances for the key proton pairs of all the linkages are reported in Table 2. For the (1→2) linkage, no NOE was detected for the H_1'–H_5 proton pair, thus indicating that the contribution of Ψ_{1-6} torsion angles far from the anti-region is indeed very minor. The J_{H5H6a} and J_{H5H6b} for the (1→6) linkage were estimated to be around 2.5 and 6.5 Hz, respectively, indicating the presence of both gg and gt conformers, the latter being predominant. From the NOESY and ROESY cross peaks and diagonal intensities at the different mixing times, no indication of distinct motion of the different branches was inferred. Indeed, the volume intensities for the key proton pairs (and H1 and H2 diagonal peaks) were very similar.

Table 2 Calculated and experimental interproton distances (Å) for **2** and the observed NOE contacts

Linkage	Proton pair	Average[b]distance (Å)	Exp. Distances (Å) (ISPA model)[c]	NOE intensity (NOE/t-ROE)	Distance (Å) for positive-Ψ/negative-Ψ conformers
α1→2	H_1'–H_1	AB[a] 3.2	AB[a] 3.3	weak	2.6/4.3
	H_1'–H_1	ED[a] 3.0	ED[a] 3.2	weak	
	H_1'–H_2	AB 2.3	AB 2.4	Strong	2.2/2.6
	H_1'–H_2	ED 2.4	ED 2.4	strong	
	H_5'–H_1	AB 2.4	AB 2.5	strong	3.6/2.3
	H_5'–H_1	ED 2.5	ED 2.6	strong-med	
α1→3	H_1'–H_3	BC[a] 2.6	BC[a] 2.3	strong	2.1/2.5
	H_1'–H_2	BC 3.8	BC 3.4	weak	2.5/4.3
	H_5'–H_2	BC 2.5	BC 2.4	medium	3.2/2.3
α1→6	H_1'–H_{6a}	DC 2.4	DC 2.5	strong	2.4–2.7
	H_1'–H_{6b}	DC 2.9	DC 3.1	weak	2.9–3.5
	H_1'–H_5	DC 4.3	not detected	not detected	4.2–4.7

[a] AB and ED stand for the two Manα1→2Man linkages, while BC and DC refer to the Manα1→3Man and Manα1→6Man linkages, respectively. In all cases, the corresponding non-reducing moiety of a given linkage is primed. For the Manα1→6Man linkage, only the Ψ 180 angle is considered.

[b] Averaged distances ($<r^{-6}>$) calculated as described in the experimental section.

[c] Distances (Å) were derived using the isolated spin-pair approximation (ISPA) according to the protocol described in the experimental section from 1D and 2D NOESY and T-ROESY data. Error estimation in the measurement are smaller than 0.2 Å.

[d] Estimated distances for the representative stacked (positive-Ψ) and extended (negative-Ψ) conformers for the Manα1→2Man, Manα1→3Man and Manα1→6Man linkages.

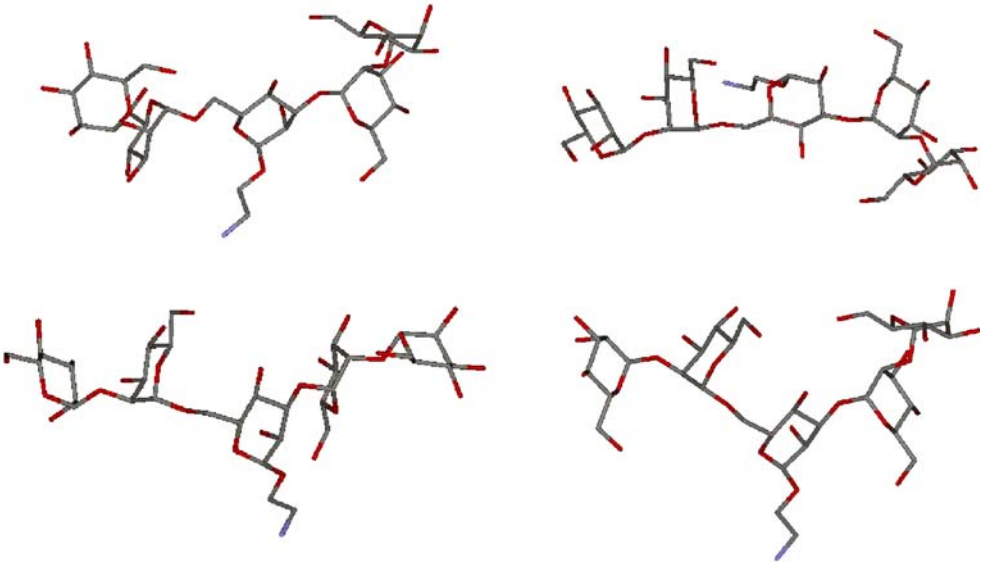

Fig. 2 The putative conformers of **2**. *Top left*. Positive Ψ values and *gt* conformation around Ψ angles. *Right*. Negative Ψ values and *gt* conformation around Ψ angles. *Bottom left*. Positive Ψ values and *gg* conformation around Ψ angles. *Right*. Negative Ψ values and *gg* conformation around Ψ angles

For both Manα1→2-Man linkages, the observed H5′–H1 NOE intensity is always more intense than the corresponding H1′–H1 (estimated distance 3.0–3.3 Å). These observations indicate that the conformational equilibrium in water solution again favours the negative-Ψ conformer over the positive one, especially for that between units A and B. The experimental NOEs account for a ca 70:30 equilibrium between the negative and positive Ψ-areas, with a slightly larger contribution of the positive-Ψ conformers for the ED fragment.

Thus, the conformational behaviour of the pentasaccharide may be described by a distribution of different geometries, which display exo-anomeric conformations around all the Φ angles of the molecule and fluctuations around the $\Psi_{1\rightarrow2}$ and $\Psi_{1\rightarrow3}$ glycosidic linkages, preferably centered around negative Ψ-values. Additional flexibility around ω at the 1→6 linkage is found. A superimposition of different representative conformers is given in Fig. 3, which also contains the superimposition of 100 snapshots from the MD simulations for both the gg and gt rotamers around ω, while the individual representations of the sixteen basic conformational families are gathered in the supporting information.

The heptasaccharide (3)

The heptasaccharide **3** shows two Manα1→2-Man additional moieties, which span out of each terminal Manα1→2-Man unit already present in **2**. Thus, **3** may be described as a composition of **1** and **2**. Indeed, now, one of the arms of **3** exactly corresponds to **1**. The manual and Monte Carlo conformational search yielded 32 conformational families within 20 kJmol^{-1} from the global minimum (Table 3). Again, these structures were used as the starting point of thirty-two separated 2 ns MD runs. The collected output of

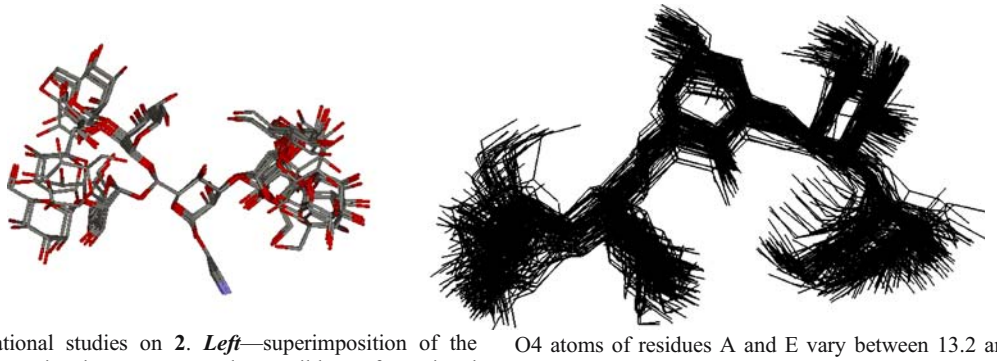

Fig. 3 Conformational studies on **2**. ***Left***—superimposition of the representative geometries that encompass the possible conformational space available to **2**. Residue C, which holds the two 1→3 and 1→6 linkages has been chosen for superimposition. Distances between the O4 atoms of residues A and E vary between 13.2 and 19.7 Å. ***Right*** superimposition of 100 snapshots taken from one of the 5 ns MD simulations starting from the gt conformer around ω

Table 3 Calculated and experimental interproton distances (Å) for **3** and observed NOE contacts

Linkage	Proton pair	Average[b] distance (Å)	Exp. distances (Å) (ISPA model)[c]	NOE intensity (NOE/t-ROE)	Distance (Å) for positive-Ψ/negative-Ψ conformers
α1→2	H_1'–H_1	AB[a] 3.2	AB[a] 3.3	weak	2.6/4.3
	H_1'–H_1	BC[a] 3.3	BC[a] 3.3	weak	
	H_1'–H_1	GF[a] 3.1	GF[a] 3.2	weak	
	H_1'–H_1	FE[a] 3.0	FE[a] 3.2	weak	
	H_1'–H_2	AB[a] 2.5	AB[a] 2.4	strong	2.2/2.6
	H_1'–H_2	BC[a] 2.4	BC[a] 2.4	strong	
	H_1'–H_2	GF[a] 2.4	GF[a] 2.4	strong	
	H_1'–H_2	FE[a] 2.5	FE[a] 2.4	strong	
	H_5'–H_1	AB[a] 2.4	AB[a] 2.6	strong-med	3.6/2.3
	H_5'–H_1	BC[a] 2.5	BC[a] 2.6	strong-med	
	H_5'–H_1	GF[a] 2.5	GF[a] 2.6	strong-med	
	H_5'–H_1	FE[a] 2.6	FE[a] 2.6	strong-med	
α1→3	H_1'–H_3	CD[a] 2.5	CD[a] 2.3	strong	2.2/2.5
	H_1'–H_2	CD[a] 3.7	CD[a] 3.3	weak	2.6/4.1
	H_5'–H_2	CD[a] 2.5	CD[a] 2.5	medium	3.2/2.3
α1→6	H_1'–H_{6a}	ED[a] 2.4	ED[a] 2.4	strong	2.4–2.7
	H_1'–H_{6b}	ED[a] 3.0	ED[a] 2.9	weak	2.9–3.5
	H_1'–H_5	ED[a] 4.3	not detected	not detected	4.2–4.7

[a] AB, BC, GF and FE are α1→2 linkages; CD, ED are α1→3, α1→6, respectively. In all cases, the corresponding non-reducing moiety of a given linkage is primed. For the 1→6, only Ψ 180 is considered.
[b] Averaged distances ($<r^{-6}>$) calculated as described in the experimental section.
[c] Distances (Å) were derived using the ISPA according to the protocol described in the experimental section. Error estimations are smaller than 0.2 Å.
[d] Estimated distances for the representative stacked (positive-Ψ) and extended (negative-Ψ) conformers.

the dynamic simulations (64 ns total simulation, Table 3) as well as the representative conformers were again compared with those obtained through NMR.

3 displays four Manα1→2-Man linkages: ManAα1-2-ManB, ManBα1-2-ManC, ManGα1-2-ManF, and ManFα1-2-ManE, (for the 1→2 arm), and ManCα1-2-ManD, and ManEα1→2-ManD (for the 1→3 and 1→6 arms, respectively). The negative Ψ conformation is preferred over the positive one, with a similar preference to that described above. The ManCα1→3-ManD also displays a similar behaviour to that detailed for **1** and **2**. The predictions for the Manα1→6-Man are also basically identical to those described for **2**. Again, for all Manα1→2-Man linkages, the H5′–H1 NOE intensity (Table 3) is more intense than the corresponding H1′–H1. These observations indicate that the conformational equilibrium in water solution favours the negative-Ψ conformers, with a estimated percentage around 75:25. The equilibrium also favours the negative (75%) over the positive Ψ values (25%) around the Cα1→3D linkage, since the experimental average C1′–D2 distance is ca. 3.3 Å, while that for C5′–D2 is 2.5 Å, in between those expected for pure Ψ positive or negative conformers.

The NOE data for the Manα1→6-Man moiety are in agreement with a basically pure Ψ anti conformation, although, as usual the calculations indicate the presence of flexibility the gg and gt rotamers around the C5–C6 linkage of unit D. The NOEs are accounted for a unique anti-Ψ conformer. Generally speaking, **3** shows an exo-anomeric conformation for Φ_{16}, with contributions from both the *gt* and *gg* conformers around ω. Again, based on the simulations, the *gg* cluster may be correlated with the presence of positive-type conformers for Ψ of the (1→2) linkage, while the Ψ_{1-6} torsion displays the anti-type conformer. The J_{H5H6a} and J_{H5H6b} for the (1→6) linkage were estimated to be around 3.0 and 5.5 Hz, respectively, indicating the presence of both gg and gt conformers. Again, from the NOESY and ROESY cross peaks and diagonal intensities at the different mixing times, no indication of differential flexibility for the two arms of **3** was deduced.

A superimposition of different representative conformers is given in Fig. 4, which also contains the superimposition of 100 snapshots from the MD simulations for both the gg and gt rotamers around ω, while individual representations of basic conformational families are gathered in the supporting information.

Therefore, these mannooligosaccharides are rather flexible molecules, and a fair amount of conformational space is available to them [38]. In principle, they could interact with a variety of mannose-binding proteins and, as a first model lectin, we decided to choose banana lectin (Banlec) [39, 40], whose 3D structure in the complex with mannose and other saccharides has been recently reported [39, 40].

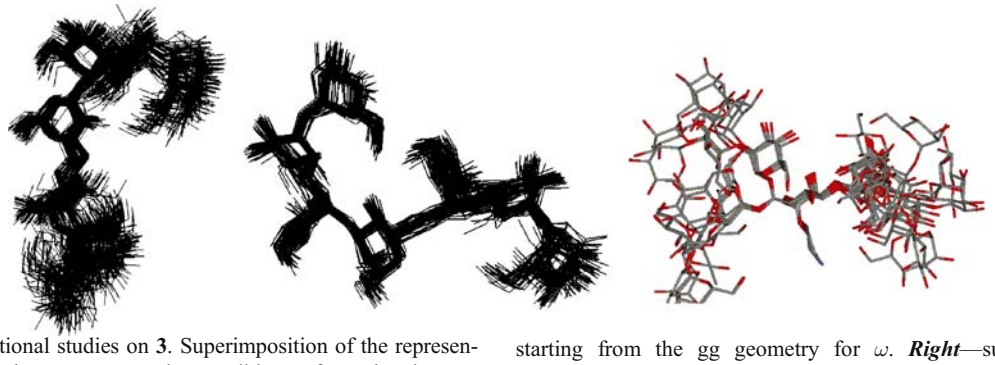

Fig. 4 Conformational studies on **3**. Superimposition of the representative geometries that encompass the possible conformational space available to **3**. ***Left***. Superimposition of 80 snapshots from the MD simulations of **3** starting from the gt geometry for ω. **Middle**. Superimposition of 80 snapshots from the MD simulations of **3** starting from the gg geometry for ω. ***Right***—superimpostion of selected structures from the MC run for **3** showing the available conformational space. Residue C, which holds the two 1→3 and 1→6 linkages has been chosen for superimposition. Distances between the O4 atoms of residues A and E vary between 9.5 and 24.0 Å

Banlec is a homodimer belongs to a subgroup of the jacalin-related lectin family that binds to glucose/mannose, but is unique in recognizing internal α1→3 as well as β1→3 linkages at the reducing termini. It has been described that presents two sugar-binding sites per monomer [39, 40].

The interaction of these mannooligosaccharides with banlec was demonstrated by using NMR [41]. In all cases, for **1**–**3**, the addition of the lectin to the NMR tubes containing the oligosaccharides induced broadening of their corresponding NMR signals.

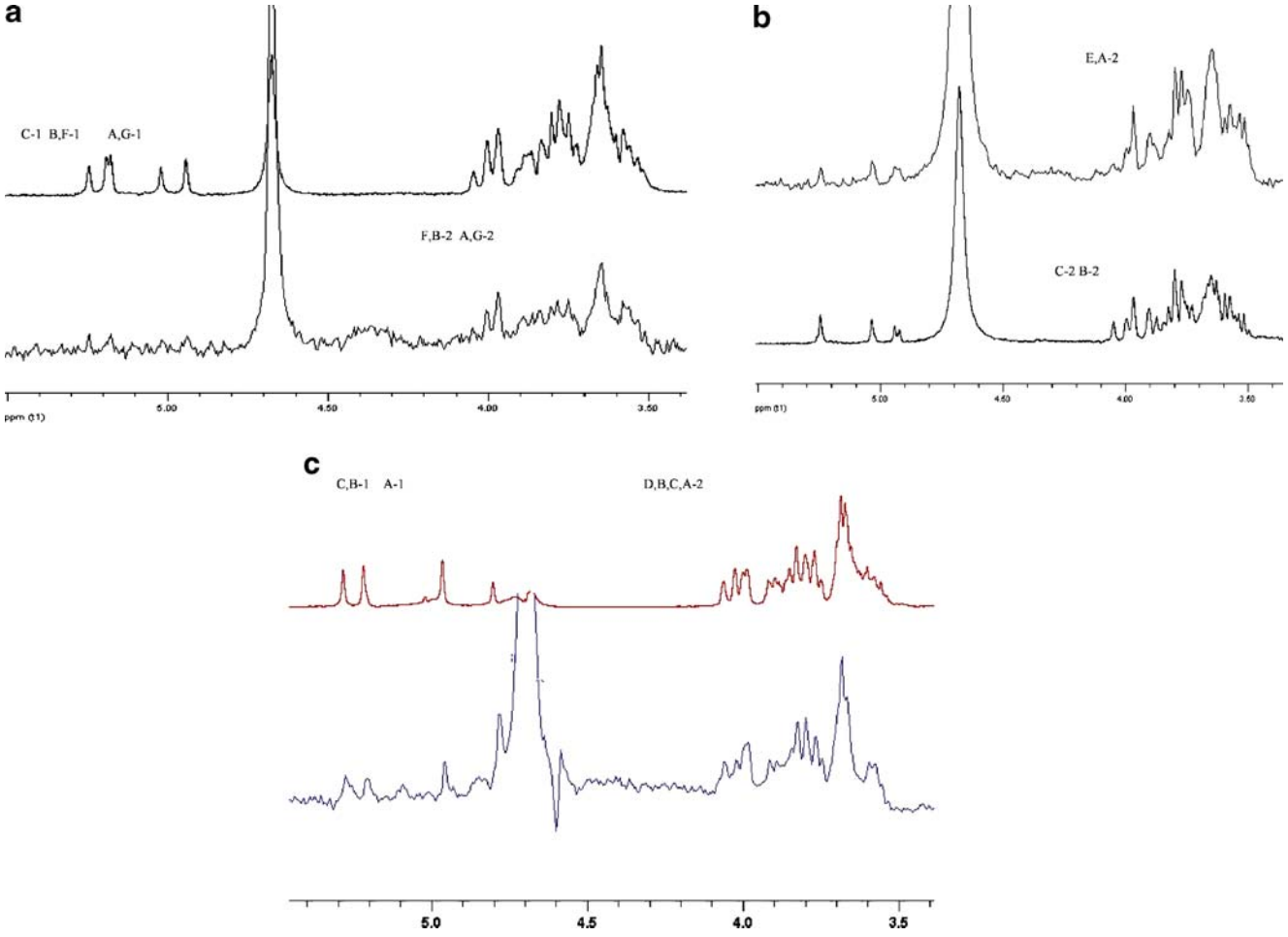

Fig. 5 STD experiments for the complexes of **a** **3**, **b** **2**, and **c** **1**, complexed to Banana lectin. The estimated molar ratio lectin/sugar is ca. 100/1. In **b** and **c**, the bottom spectra are the regular 1D 1H NMR of the sugar in the presence of the lectin. The top spectra are the corresponding STD responses after saturating for 2 s at δ—1 ppm. In all cases, the highest response is at the terminal units, especially for H-2

Table 4 Estimated STD intensities for the complexes of **1**–**3** with Banana lectin

Atom	ManA	ManB	ManC	ManD			
H-1 (%)	70	50	50	–			
H-2 (%)	100	60	60	80			
Atom	ManA	ManB	ManE	ManD	ManC		
H-1 (%)	45	25	45	30	–		
H-2 (%)	100	45	100	75	2		
Atom	ManA	ManB	ManC	ManD	ManE	ManF	ManG
H-1 (%)	20	20	15	–	8	20	20
H-2 (%)	100	60	60	25	35	60	100

The estimated molar ratio lectin/sugar is ca. 100/1. STD responses were measured after saturating for 2 s at δ—1 ppm). In each case, the intensities are normalized at the highest response, which corresponds to one of the H-2 protons. For **1**, the highest STD intensity is observed at the non-reducing end, residue A, followed by that at D seems also be high, although is partially obscured by the residual water signal. For **2**, the highest response is observed at both terminal non-reducing ends, A and E. For **3**, the highest response is again at both terminal non-reducing ends.

STD experiments were then used to further ascertain the interaction [42, 43]. The corresponding spectra are given in Fig. 5. In each case, the intensities are normalized (Table 4) at the highest response, which always corresponded to one of the H-2 protons, especially belonging to the non-reducing ends. This fact may indicate the direct involvement of the H-2 region of the non-reducing ends in the binding to the lectin (see below).

For **1**, clear STD effects for all the H-2 protons were deduced. The STD effects were smaller for the anomeric signals. The highest STD intensity was observed at the non-reducing end, residue A, followed by that at D. This fact may indicate that the binding event takes place preferentially around these non-reducing residues. Especially, the H-2 protons received the highest saturation, probably indicating major binding through O-2. The different STD effects at H-2 and H-1 (Table 4) are probably due to their different orientation in the pyranose ring, also in agreement with the fact that the intensities at the H-3 region are also higher than for H-1. The percentages of STD intensities are given in Table 4.

For pentasaccharide **2**, the highest response is observed at both terminal non-reducing ends, A and E. Indeed, as for **1**, major STDs are observed for both H-2 signals of the external residues.

The STD for the **3**/banlec sample shows the highest response at both non-reducing ends. Again, major enhancements for H-2s of the more external 1→2 linked residues and minor enhancements for the anomeric protons.

Although attempts for crystallization and further NMR experiments are presently being carrying out in our laboratories, by using docking procedures, we have performed a preliminary docking analysis of the possible binding modes of **1**–**3** to banlec [44].

First, the possibility of every saccharide to simultaneously access the two binding sites at a given monomer was evaluated. For that, the different possible conformations in solution were considered.

From the X-ray structure of each of the monomers of banlec when complexed to two mannose moieties, the distance between the two O-4 atoms of the bound sugars

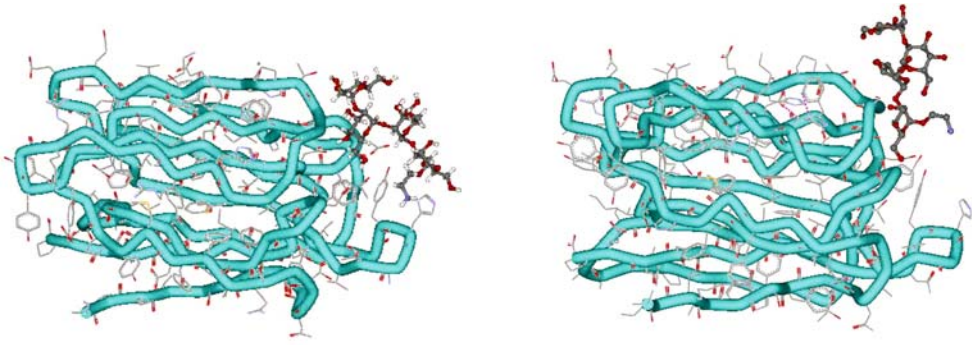

Fig. 6 The two more plausible modes of interaction of tetrasaccharide **1** with banana lectin, according to docking simulations and STD experiments. Either the reducing or non-reducing moieties of **1** may be docked at either binding site without major steric conflicts. The STD spectrum show all H-2s with high intensity

ranges between 13 and 14 Å. For **1**, the distance between the O-4 atoms of residues A and D oscillates between 7 and 11 Å, depending on the conformation around Φ/Ψ of both 1→2 and 1→3 linkages. Therefore, there are no possibilities for one tetrasaccharide entity being simultaneously bound to both binding sites. The possibility of docking every mannose residue to each of the two binding sites was then explored. It was deduced that either both terminal Man residues (either the reducing or non-reducing ones) may be docked at both binding sites without major steric conflicts. The other oligosaccharide may point out of the binding site or provide additional contacts with the protein surface (Fig. 6). Regarding the internal residues, only residue B might also produced a positive docking model, but only at one of the binding sites, while the binding of residue C seems to be forbidden by steric conflicts. The putative binding modes are given in the supporting information. The STD experiments point toward major binding through the non-reducing end, in better qualitative agreement with one of the binding modes shown in Fig. 6 (left).

For the pentasaccharide, the distance between the two *O*-4 atoms of the 1→2 linked terminal residues ends oscillate between 13 and 20 Å, thus producing the possibility of simultaneous binding to the two Man-binding sites. Indeed, for the gg conformer around the 1→6 linkage, and the two 1→2 and the 1→3 linkages adopting the more stable negative-Ψ conformations, there is possibility of simultaneous binding, as shown in Fig. 7. However, in this branched case, the reducing moiety cannot be docked in any of the binding sites without producing major steric conflicts between one of the arms and the protein. Only the possibility of binding the non-reducing terminal Man moieties indeed occur. The STD experiment shows their H-2s with enhanced intensity with respect to the others in qualitative agreement with this model.

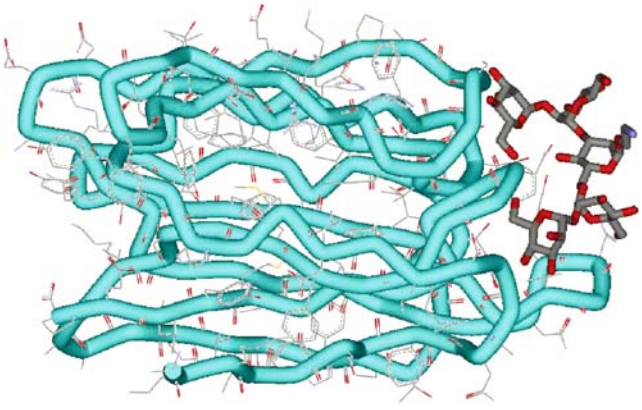

Fig. 7 Docking of pentasaccharide **2** at banana lectin binding site. The two non-reducing mannose moieties at both 1→3 and 1→6 arms can be docked simultaneously at both binding sites. The STD experiment shows their H-2s with enhanced intensity with respect to the others

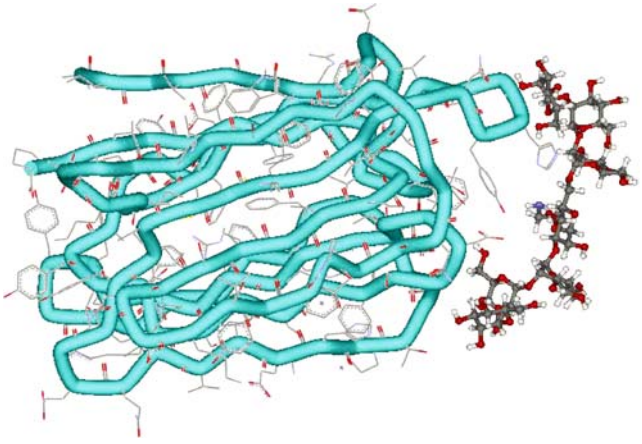

Fig. 8 One of the plausible modes of interaction of heptasaccharide **3** with banana lectin. Either non-reducing moiety of **3** may be docked at either binding site without major steric conflicts. The STD spectrum show the H-2s of the mannose moieties occupying the non-reducing ends with the highest intensity

For the heptasaccharide, the distance between both *O*-4 atoms of the two terminal Man residues oscillates between 10 and 24.0 Å, but now simultaneous binding of two terminal mannoses is not a possible solution for the major conformations around the glycosidic linkages. However, independent binding of any of them is allowed without major steric conflicts (Fig. 8). On the other hand, binding the internal Man1→2 linked residue belonging to the 1→3 arm may also take place, providing a satisfactory docking solution. Nevertheless, the STD intensities are in qualitative agreement with those solutions that predict interaction of the non-reducing ends with the lectin, as that shown in Fig. 8.

In all cases, for **1**–**3** a variety of intermolecular lectin-sugar hydrogen bonds and van der Waals contacts provide the stability for the complex formation. These are basically equivalent to those already described [39, 40].

Therefore, according to the docking studies, several solutions are accessible for binding of these oligosaccharides to banlec. Moreover, different binding modes of the three saccharides to the same lectin are probably occurring. In any case, the STD experiments allow deducing that the three oligosaccharides effectively interact with this lectin and that they may be used for elaboration to allow their multivalent presentation (See Appendix). Further studies are taking place in our labs to explore these possibilities.

Acknowledgments We thank the EU (grant LSHP-CT2003-503558), the Ministry of Education and Science of Spain for funding (CTQ2006-10874-C02-01 (to JJB) and CTQ2005-07993-C02-01 (to SP), as well as grants from the Department of Science and Technology and the Department of Biotechnology, Government of India to A. S. We also thank Dr. A. Olson (Scripps Research Institute, USA) for providing the Auto-Dock and auxiliary programs.

Appendix

Supporting Information

Table 5 1H and 13C NMR Chemical shifts for compounds **1**–**3**

Compound **1**

Atom	ManA	ManB	ManC	ManD	Atom	ManA	ManB	ManC	ManD
H-1	4.97	5.23	5.29	4.81	C-1	102.2	100.6	100.7	99.8
H-2	3.99	4.03	4.00	4.06	C-2	69.9	78.5	78.6	69.4
H-3	3.76	3.87	3.91	3.84	C-3	70.3	70.0	70.0	78.5
H-4	3.56	3.61	3.62	3.69	C-4	66.8	67.0	66.9	65.9
H-5	3.67	3.66	3.68	3.59	C-5	73.2	73.2	73.2	73.1
H-6[a]	3.82	3.81	3.80	3.83	C-6	60.8	60.9	60.8	60.9
H-6B	3.68	3.67	3.69	3.68					

Compound **2**

Atom	ManA	ManB	ManE	ManD	ManC
H-1	4.98	5.29	4.96	5.08	4.79
H-2	4.00	4.03	4.00	3.94	4.07
H-3	3.77	3.92	3,78	3.87	3.83
H-4	3.57	3.61	3.57	3.62	3.82
H-5	3.68	3.69	3.69	3.61	3.72
H-6[a]	3.82	3.81	3.82	3.83	3.92
H-6B	3.68	3.68	3.69	3.68	3.64
Atom	ManA	ManB	ManE	ManD	ManC
C-1	102.2	100.8	102.3	97.9	100.0
C-2	69.9	78.5	69.9	78.7	69.4
C-3	70.3	70.0	70.3	70.2	78.9
C-4	66.8	66.9	66.8	66.9	65.4
C-5	73.3	73.2	73.2	72.7	71.3
C-6	60.9	61.0	61.0	60.9	65.3

Compound **3**

Atom	ManA	ManB	ManC	ManD	ManE	ManF	ManG
H-1	4.97	5.23	5.29	4.79	5.06	5.21	4.97
H-2	4.00	4.03	4.03	4.07	3.94	4.03	4.00
H-3	3.77	3.87	3.92	3.83	3.87	3.87	3,78
H-4	3.57	3.61	3.61	3.82	3.62	3.61	3.57
H-5	3.68	3.66	3.69	3.72	3.61	3.66	3.69
H-6[a]	3.82	3.81	3.81	3.92	3.83	3.81	3.82
H-6B	3.68	3.67	3.68	3.64	3.68	3.67	3.69
Atom	ManA	ManB	ManC	ManD	ManE	ManF	ManG
C-1	102.2	100.6	100.8	100.0	97.9	100.6	102.3
C-2	69.9	78.5	78.5	69.4	78.7	78.5	69.9
C-3	70.3	70.0	70.0	78.9	70.2	70.0	70.3
C-4	66.8	67.0	66.9	65.4	66.9	67.0	66.8
C-5	73.3	73.2	73.2	71.3	72.7	73.2	73.2
C-6	60.9	60.9	61.0	65.3	60.9	60.9	61.0

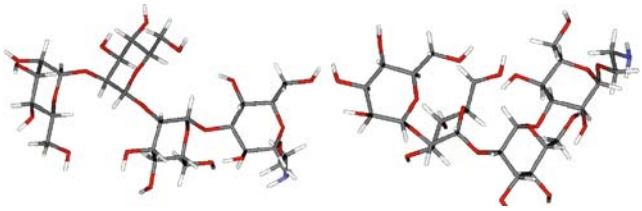

The two major putative conformers according to MM3* calculations. Left, negative Ψ values. Right, positive Ψ values.

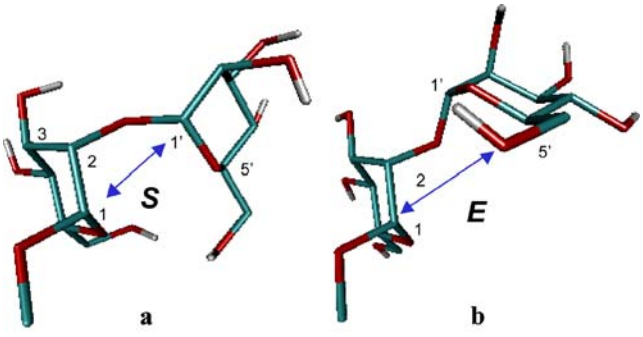

Representative low-energy conformations of Manα1→2-Man of **1. a** The positive (stacked, S) Ψ conformation (Φ, Ψ −33°, 57°); **b** The negative (extended, E) Ψ conformation (Φ, Ψ −55°, −22°). Characteristic NOE contacts are indicated by the blue arrows. In both cases, there is close proximity for the H1′–H2 proton pair.

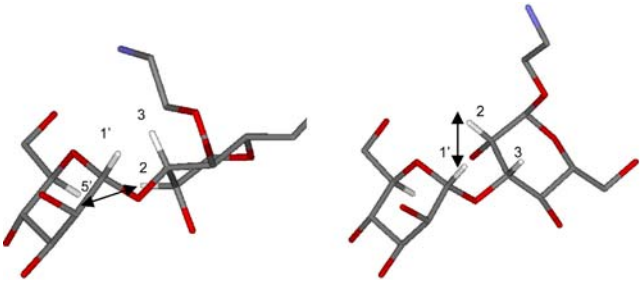

Representative low-energy conformations of Manα1→3-Man (a, b) of **1. Left** The positive Ψ conformation (Φ, Ψ −33°, 45°); **Right** The negative Ψ conformation (Φ, Ψ −58°, −16°). Characteristic NOE contacts are indicated by the blue arrows. In both cases there is close proximity for the H1′–H3 proton pair.

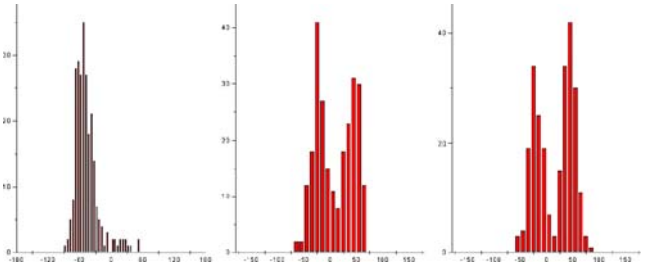

Conformational studies on the (1→2) and (1→3) linkages of **1**. $\Phi_{1\to2}$: H1′–C1′–O–C2; $\Psi_{1\to2}$: C1′–O–C2–H2. $\Phi_{1\to3}$: H1′–C1′–O–C3; $\Psi_{1\to3}$: C1′–O–C3–H3. Calculations were run with MMOD 7.0, using MM3* and the GB/SA water solvation model. **Left** Variations of Ψ during the 5 ns of MD simulation on the (1→3) linkage. Negative Ψ values are very predominant. **Middle** Variations of Ψ during one of the 5 ns MD simulations on the (1→2) linkage for the BC fragment, starting from positive Ψ. Equilibrium between positive and negative Ψ values is evident. **Right** Variations of Ψ during the 5 ns of MD simulation on the (1→2) linkage for the AB fragment starting from positive Ψ. Equilibrium between positive and negative Ψ values is evident. In both cases, when the starting conformer is the negative Ψ geometry, this is the predominant one.

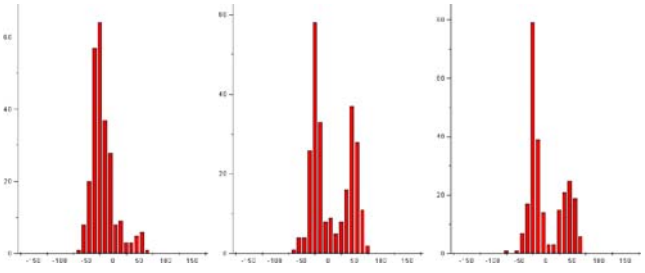

Left Variations of $\Psi_{1\to3}$ during the 5 ns of MD simulation on the (1→3) linkage. The negative Ψ area is strongly predominant. **Middle** Variations of $\Psi_{1\to3}$ during the 5 ns of MD simulation on the (1→2) linkage for the BC fragment starting from positive Ψ. The equilibrium around Ψ is evident, with predominance of the negative values. **Right** Variations of $\Psi_{1\to3}$ during the 5 ns of MD simulation on the (1→2) linkage for the AB fragment starting from positive Ψ. The equilibrium around Ψ is evident, with predominance of the negative values.

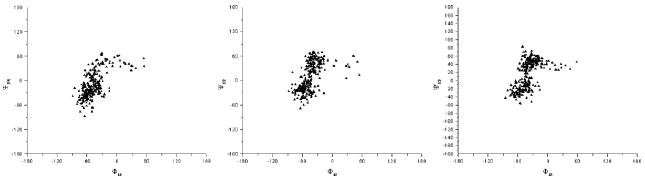

Left Variations of Φ/Ψ during the 5 ns of MD simulation on the (1→3) linkage. Negative Ψ values are strongly predominant. **Middle** Variations of Φ/Ψ during the 5 ns of MD simulation on the (1→2) linkage for the AB mannobiose fragment starting from positive Ψ. The equilibrium between the positive and negative Ψ values is evident. **Right** Variations of Φ/Ψ during the 5 ns of MD on the (1→2) linkage for the GF fragment starting from positive Ψ. The equilibrium between positive and negative Ψ values is evident.

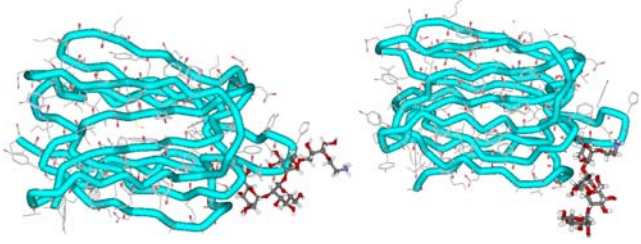

Two additional modes of interaction of tetrasaccharide **1** with banana lectin, according to docking simulations and STD experiments. Either the reducing or non-reducing moieties of **1** may be docked at either binding site without major steric conflicts. The STD spectrum show all H-2s with high intensity.

Different conformers of heptasaccharide 3, as predicted by MM3*-based Monte Carlo calculations

Top panel

The twelve more stable conformers produced by changes in Ψ angles around the different 1→2 and 1→3 glycosidic linkages, while maintaining a *gt* conformer around ω.

The two superimpositions show the accesible conformational space, while maintaining a *gt* conformer around ω, and flexibility around the 1→2 glycosidic linkages.

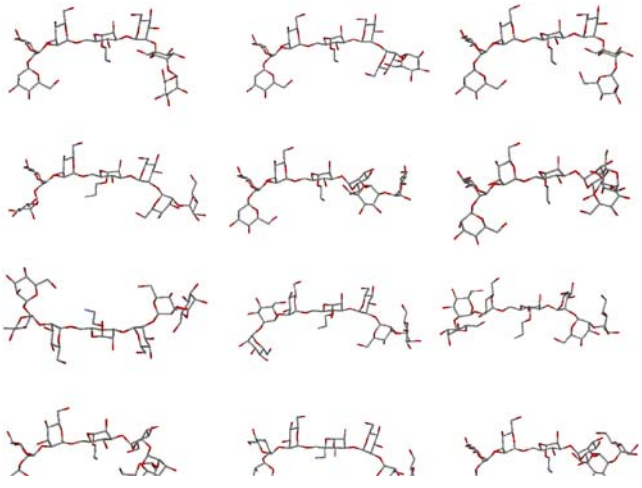

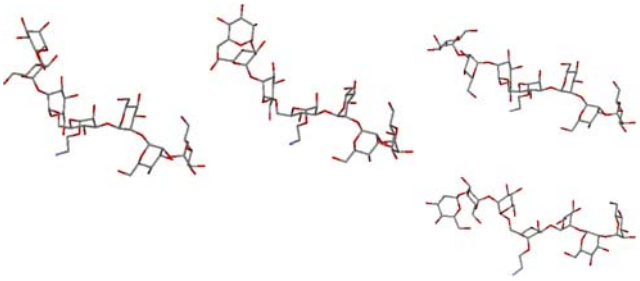

Bottom panel

The four more stable conformers produced by changes in Ψ angles around the different 1→2 and 1→3 glycosidic linkages, while maintaining a *gg* conformer around ω.

The superimposition at the bottom show the conformational space accesible for both *gg* and *gt* conformers around ω, while keeping the same conformation around the 1→3 arm and flexibility around the two 1→2 glycosidic linkages at the 1→6 arm.

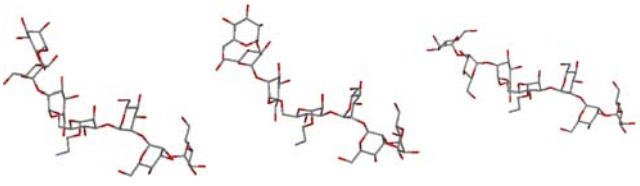

Different conformers of pentasaccharide 2, as predicted by MM3*-based Monte Carlo calculations

A.–The four more stable conformers produced by changes in Ψ angles around the different 1→2 and 1→3 glycosidic linkages, while maintaining a *gt* conformer around ω.

B.–Superimpositions showing the accessible conformational space, while maintaining a gt conformer around ω, and flexibility around the 1→2 and 1→3 glycosidic linkages.

C.– The superimposition at the bottom show the conformational space accesible upon motion at the terminal end of the 1→6 arm. Left.– For the gt conformer around ω Right: For both *gt* and *gg* conformers around ω.

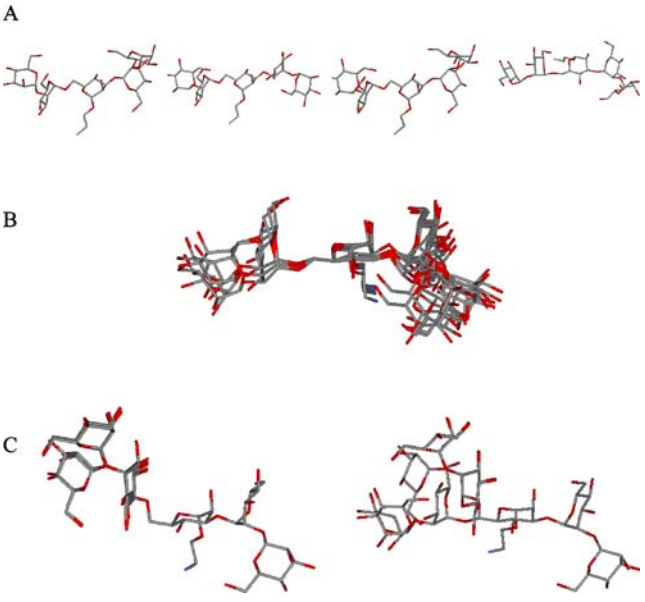

The different conformers of **1**, as predicted by MM3*-based Monte Carlo calculations

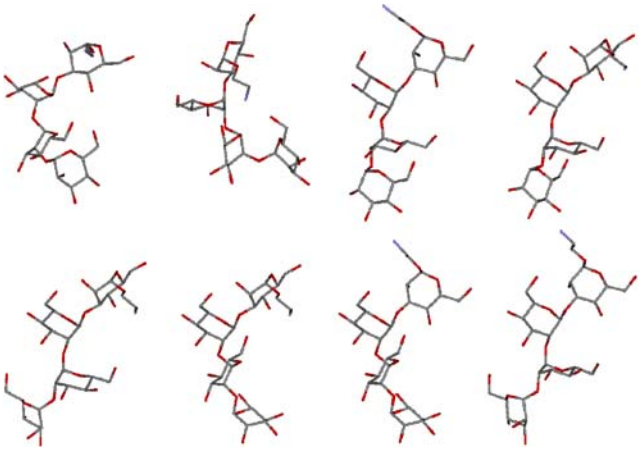

The eight more stable conformers produced by changes in Ψ angles around the different 1→2 and 1→3 glycosidic linkages.

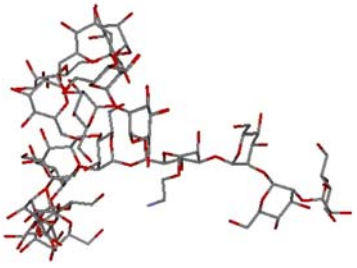

References

1. Gabius, H.-J., Siebert, H.-C., Andre, S., Jimenez-Barbero, J., Rudiger, H.: Chemical biology of the sugar code. ChemBioChem **5**, 740–764 (2004)
2. Ito, Y., Hagihara, S., Matsuo, I., Totani, K.: Structural approaches to the study of oligosaccharides in glycoprotein quality control. Curr. Opin. Struck. Biol. **15**, 481–489 (2005)
3. Botos, I., Wlodawer, A.: Proteins that bind high-mannose sugars of the HIV envelope. Prog. Biophys. Mol. Biol. **88**, 233–282 (2005)
4. See, for instance, Lam, S.N., Gervay-Hague, J.: Glycal scavenging in the synthesis of disaccharides using mannosyl iodide donors. J. Org. Chem. **70**, 2387–2390 (2005)
5. Mandal, M., Dudkin, V.Y., Geng, X., Danishefsky, S.: In pursuit of carbohydrate-based HIV vaccines, Part 1: the total synthesis of hybrid-type gp120 fragments. Angew. Chem., Int. Ed. **43**, 2557–2561 (2004)
6. Kiessling, L., Pontrello, J.K., Schuster, M.C.: Synthetic multivalent carbohydrate ligands as effectors or inhibitors of biological processes. In: Wong, C.-H. (ed.) Carbohydrate-based Drug Delivery, pp. 575–609. Wiley-VCH, Weinheim (2003)
7. Wang, L.X., Ni, J., Singh, S., Li, H.: Binding of high-mannose-type oligosaccharides and synthetic oligomannose clusters to human antibody 2G12: implications for HIV-1 vaccine design. Chem. Biol. **11**, 127 (2004)
8. Barrientos, A.G., De la Fuente, J.M., Rojas, T.C., Fernández, A., Penadés, S.: Gold glyconanoparticles: synthetic polyvalent ligands mimicking glycocalyx-like surfaces as tools for glycobiological studies. Chem. Eur. J. **9**, 1909–1921 (2003)
9. De la Fuente, J.M., Barrientos, A.G., Rojas, T.C., Rojo, J., Fernández, A., Penadés, S.: Gold glyconanoparticles as water-soluble polyvalent models to study carbohydrate interactions. Angew. Chem., Int. Ed. **40**, 2257–2261 (2001)
10. de Souza, A.C., Halkes, K.M., Meeldijk, J.D., Verkleij, A.J., Vliegenthart, J.F.C., Kamerling, J.P.: Gold glyconanoparticles as probes to explore the carbohydrate-mediated self-recognition of marine sponge cells. ChemBioChem **6**, 828–831 (2005)
11. Rojo, J., Díaz, V., de la Fuente, J., Segura, I., Barrientos, A.G., Riese, H.H., Bernad, A., Penadés, S.: Gold glyconanoparticles as new tools in antiadhesive therapy. ChemBioChem **5**, 291–297 (2004)
12. Kogelberg, H., Solís, D., Jiménez-Barbero, J.: New structural insights into carbohydrate-protein interactions from NMR spectroscopy. Curr. Opin. Struck. Biol. **13**, 646–653 (2003)
13. De la Fuente, J.M., Penadés, S.: Glyconanoparticles: types, synthesis and applications in glycoscience, biomedicine and material science. Biochim. Biophys. Acta **1760**, 636–651 (2006)
14. Singh, D.D., Saikrishnan, K., Kumar, P., Dauter, Z., Sekar, K., Surolia, A., Vijayan, M.: Purification, crystallization and preliminary X-ray structure analysis of the banana lectin from Musa paradisiacal. Acta Crystallogr., D **60**, 2104–2106 (2004)
15. Goldstein, I.J.: Lectin structure-activity: the story is never over. J. Agric. Food Chem. **50**, 6583–6585 (2002)
16. Lee, H.-K., Scanlan, C.N., Huang, C.-Y., Chang, A.Y., Calarese, D.A., Dwek, R.A., Rudd, P.M., Burton, D.R., Wilson, I.A., Wong, C-H.: Reactivity-based one-pot synthesis of oligomannoses: defining antigens recognized by 2G12, a broadly neutralizing anti-HIV-1 antibody. Angew. Chem., Int. Ed. **43**, 1000–1003 (2004)
17. Bax, A., Davis, D.G.: MLEV-17 based two-dimensional homonuclear magnetization transfer spectroscopy. J. Magn. Reson. **65**, 355–360 (1985)
18. Kumar, A., Ernst, R.R., Wüthrich, K.: A two-dimensional nuclear overhauser enhancement (2D NOE) experiment for the elucidation

of complete proton–proton cross-relaxation networks in biological macromolecules. Biochem. Biophys. Res. Commun. **95**, 1–6 (1980)
19. Hwang, T.L., Shaka, A.J.: Cross relaxation without TOCSY: transverse rotating-frame overhauser effect spectroscopy. J. Am. Chem. Soc. **114**, 3157–3158 (1992)
20. Bodenhausen, G., Reuben, D.J.: Natural abundance nitrogen-15 NMR by enhanced heteronuclear spectroscopy. Chem. Phys. Lett. **69**, 185–189 (1980)
21. Stott, K., Stonehouse, J., Keeler, J., Hwang, T.L., Shaka, A.J.: Excitation sculpting in high-resolution nuclear magnetic resonance spectroscopy: application to selective NOE experiments. J. Am. Chem. Soc. **117**, 4199–4200 (1995)
22. See, for instance, Asensio, J.L., Cañada, F.J., Khan, N., Mootoo, D.A., Jiménez-Barbero, J.: Conformational differences between O- and C-glycosides: the α-O-Man-(1→1)-β-Galα/-C-Man-(1→1)-β-Gal case—a decisive demonstration of the importance of the exo-anomeric effect on the conformation of glycosides. Chem. Eur. J. **6**, 1035–1041 (2000)
23. Mayer, M., Meyer, B.: Group epitope mapping by saturation transfer difference NMR to identify segments of a ligand in direct contact with a protein receptor. J. Am. Chem. Soc. **123**, 6108–6117 (2001)
24. Mohamadi, F., Richards, N.G.J., Guida, W.C., Liskamp, R., Lipton, M., Caufield, C., Chang, G., Hendrickson, T., Still, W.C.: MacroModel—an integrated software system for modeling organic and bioorganic molecules using molecular mechanics. J. Comput. Chem. **11**, 440–467 (1990)
25. Allinger, N.L., Yuh, Y.H., Lii, J.H.: Molecular mechanics. The MM3 force field for hydrocarbons 1. J. Am. Chem. Soc. **111**, 8551–8566 (1989)
26. Still, W.C., Tempzyk, A., Hawley, R., Hendrickson, T.: Semianalytical treatment of solvation for molecular mechanics and dynamics. J. Am. Chem. Soc. **112**, 6127–6129 (1990)
27. Perez, S., Imberty, A., Engelsen, S., Gruza, J., Mazeau, K., Jimenez-Barbero, J., Poveda, A., Espinosa, J.F., van Eyck, B.P., Johnson, G., et al.: A comparison and chemometric analysis of several molecular mechanics force fields and parameter sets applied to carbohydrates. Carbohydr. Res. **314**, 141–155 (1998)
28. Woods, R.J., Pathiaseril, A., Wormald, M.R., Edge, C.J., Dwek, R.A.: The high degree of internal flexibility observed for an oligomannose oligosaccharide does not alter the overall topology of the molecule. Eur. J. Biochem. **258**, 372–386 (1998)
29. Gonzalez, L., Solis, D., Diaz-Mauriño, T., Bruix, M., Rico, M., Feizi, T., Jiménez-Barbero, J.: Conformational studies of the man8 oligosaccharide on native ribonuclease b and on the reduced and denatured protein. Arch. Biochem. Biophys. **383**, 17–27 (2000)
30. Bernardi, A., Colombo, A., Sanchez-Medina, I.: Conformational analysis and dynamics of mannobiosides and mannotriosides using Monte Carlo/stochastic dynamics simulations. Carbohydr. Res. **339**, 967–973 (2004)
31. Mari, S., Posteri, H., Marcou, G., Potenza, D., Micheli, F., Canada, F.J., Jimenez-Barbero, J., Bernardi, A.: Synthesis, conformational studies and mannosidase stability of a mimic of 1,2-mannobioside. Eur. J. Org. Chem. **24**, 5119–5225 (2004)
32. Edge, C.J., Singh, U.C., Bazzo, R., Taylor, G.L., Dwek, R.A., Rademacher, T.W.: 500-Picosecond molecular dynamics in water of the Man.alpha.1 .fwdarw. 2Man.alpha. glycosidic linkage present in Asn-linked oligomannose-type structures on glycoproteins. Biochemistry **29**, 1971–1974 (1990)
33. Almond, A., Bunkenborg, J., Franch, T., Gotfredsen, C.H., Duus, J.O.: Comparison of aqueous molecular dynamics with NMR relaxation and residual dipolar couplings favors internal motion in a mannose oligosaccharide. J. Am. Chem. Soc. **123**, 4792–4802 (2001)
34. Rutherford, T.J., Partridge, J., Weller, C.T., Homans, S.W.: Characterization of the extent of internal motions in oligosaccharides. Biochemistry **32**, 12715–12724, (1993)
35. Almond, A., Duus, J.: Quantitative conformational analysis of the core region of N-glycans using residual dipolar couplings, aqueous molecular dynamics, and steric alignment. J. Biomol. NMR **20**, 351–363 (2001)
36. Neuhaus, D., Williamson, M.P.: The Nuclear Overhauser Effect in Structural and Conformational Analysis. VCH, New York (1989)
37. Woods, R.J., Edge, C.J., Dwek, R.A.: Protein surface oligosaccharides and protein function. Nat. Struct. Mol. Biol. **1**, 499–501 (1994)
38. Naidoo, K.J., Denysyk, D., Brady, J.W.: Molecular dynamics simulations of the N-linked oligosaccharide of the lectin from Erythrina corallodendron. Protein Eng. **10**, 1249–1261 (1997)
39. Singh, D.D., Saikrishnan, K., Kumar, P., Surolia, A., Sekar, K., Vijayan, M.: Unusual sugar specificity of banana lectin from Musa paradisiaca and its probable evolutionary origin. Crystallographic and modelling studies. Glycobiology **15**, 1025–1032 (2005)
40. Meagher, J.L., Winter, H.C., Ezell, P., Goldstein, I.J., Stuckey, J.A.: Crystal structure of banana lectin reveals a novel second sugar binding site. Glycobiology **15**, 1033–1042 (2005)
41. Jiménez-Barbero, J., Peters, T.: NMR Spectroscopy of Glycoconjugates. VCH, Weinheim (2002)
42. Jayalakshmi, V., Biet, T., Peters, T., Krishna, N.R.: Refinement of the conformation of UDP-Galactose bound to galactosyltransferase using the STD NMR intensity-restrained CORCEMA optimization. J. Am. Chem. Soc. **126**, 8610–8611 (2004)
43. Mari, S., Serrano-Gómez, D., Cañada, F.J., Corbí, A.L., Jiménez-Barbero, J.: 1D saturation transfer difference NMR Experiments on living cells: the DC-SIGN/Oligomannose interaction. Angew. Chem., Int. Ed. **44**, 296–298 (2005)
44. Asensio, J.L., Espinosa, J.F., Dietrich, H., Cañada, F.J., Schmidt, R.R., Martin-Lomas, M., André, S., Gabius, H-J., Jiménez-Barbero, J.: Bovine heart galectin-1 selects a unique (Syn) conformation of C-lactose, a flexible lactose analogue. J. Am. Chem. Soc. **121**, 8995–9000 (1999)